This article has been accepted for publication in a future issue of this journal, but has not been fully edited. Content may change prior to final publication. Citation information: DOI 10.1109/ACCESS.2017.2727502, IEEE Access

Hybrid Vision Based Reach-to-Grasp Task Planning Method for Trans-humeral Prostheses

D.G. Kanishka Madusanka, R.A.R.C. Gopura, Y.W.R. Amarasinghe, G.K.I. Mann

***Abstract*—This paper proposes a hybrid vision based reach-to-grasp task planning method for trans-humeral prostheses exploiting both vision and Electromyography (EMG) signals. The hybrid method mainly consists of 2-1/2D visual servoing module and EMG based module. The visual servoing intends to align the object on to the center of the palm while correcting its orientation. EMG signals extracted from the remaining muscles of the disabled arm due to amputation are used to control the elbow flexion/extension (FE). While using the 2-1/2D visual servoing module, the object reaching algorithm changes the elbow FE angle to reach the palm towards the object of interest. Initially, the EMG based module controls the elbow FE. Once an object is detected, the EMG signals emanating from the arm muscles generates a reach request. This process then activates the visual servoing module to bring the palm towards the object. Since both EMG based module and the visual servoing module are producing elbow FE angles while reaching towards an object, these two modules are integrated to obtain a resultant angle for elbow FE. Experiments are conducted using a simulation environment and a prosthesis to validate the proposed task planning method. The EMG based module is capable of following the natural elbow FE motion. Moreover, the task planning method is capable of driving the prosthesis towards the object with proper orientation.**

***Index Terms*—Prosthesis, Electromyography, 2-1/2D visual servoing**

I. Introduction

LOSS of the upper limb leaves an amputee unable to realize even the most basic activities of daily living (ADL). Full or partial loss of the upper limb can occur due to diseases, trauma, accidents, etc. [1]. Researchers are consistently focusing their efforts towards developing functional and reliable prostheses to uplift the living standards of amputees [2]–[6]. The ultimate objective of such research is to develop a prosthesis which accurately mimics the characteristics and functionality of their biological counterparts.

In most circumstances, biological signals are used to control externally powered prostheses. Electromyography (EMG) [7], [8], Electroencephalography (EEG) [9], and Electrocorticography (ECoG) [10] are some of the commonly used biological signals. Among these biological signals, EMG is preferred by researchers due to its advantages such as higher signal to noise ratio and ease of extraction [11], [12].

EMG signals can be easily extracted from the surface of the muscles, i.e. surface EMG [7], [13]. However, due to amputations, many muscles are unavailable for extracting EMG signals. For example, after a trans-humeral amputation, only parts of the biceps brachii and triceps brachii are available. All other muscles below the point of amputation are lost. In order to regain lost muscle signals, a surgical procedure known as Targeted Muscle Reinnervation (TMR) is performed [14], [15]. However, due to the invasiveness of the required surgery, risks such as phantom limb pain and permanent paralysis of innervated muscles are associated with TMR process [14]. Moreover, amputees may refuse to undergo a surgery. As a solution to the problem, researchers are integrating different external sensory inputs with EMG signals to control prostheses [2], [12]. These systems are referred to as hybrid myoelectric control systems [2]. The recent addition to control prostheses are vision sensors [2], [16]. Due to the amputation, the link between the upper limb and the human vision system fails [2]. As a solution to this broken link, vision sensors can be used to get inputs to the prosthetic controller and hence give vision capabilities.

Visual servoing is the use of vision feedback as a control input [17]–[19]. Visual servoing can be carried out in different methods using different camera placements [20]. Eye-in-hand camera configuration method can be used for a prosthesis application where the system can be mobile and independent of the environment. However, if stationary fixed cameras are used the user must be within the view of the camera to operate the prosthesis.

Few vision based prosthetic controllers are reported in literature, which are listed in Table I. Majority of research carried out by integrating vision sensors to control upper limb prostheses are conducted to control trans-radial prostheses [16], [21]–[24]. In which, wrist and hand motions are performed with the aid of vision [21]–[23] and in some of them EMG is used only as a trigger to open and close the hand [16], [21]. Only the orientation of hand is corrected in those prostheses to reach towards an object of interest [22], [24]. This has been achieved by directly calculating the required rotation angle from image data in [24], and using an accelerometer in [22]. However, reach-to-grasp task of a trans-humeral prosthesis requires the palm to be moved closer to the object and correct the orientation of palm according to the user intention. In order to achieve that, vision signals and EMG signals should be integrated. Therefore in this research a hybrid vision based task planning method integrating vision

*This work was supported by Senate Research Council (SRC) grant (no. SRC/LT/2013/07)

D.G. Kanishka Madusanka, and R.A.R.C. Gopura are with the Bionics Laboratory, Department of Mechanical Engineering, University of Moratuwa, Sri Lanka. {kanishkaM, gopura} @ieee.org

Y.W.R. Amarasinghe is with the Department of Mechanical Engineering, University of Moratuwa, Sri Lanka. ranamajp@gmail.com

G.K.I. Mann is with the Faculty of Engineering and Applied Science, Memorial University of Newfoundland, Newfoundland, Canada. gmann@mun.ca

This article has been accepted for publication in a future issue of this journal, but has not been fully edited. Content may change prior to final publication. Citation information: DOI 10.1109/ACCESS.2017.2727502, IEEE Access

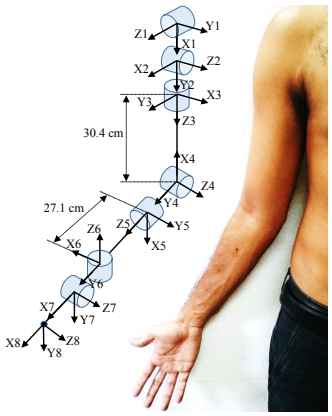

Fig. 1. Kinematic structure of upper limb. Coordinate frames from frame 1 ($[X1, Y1, Z1]$) to frame 8 are assigned with shoulder AAD, shoulder FE, shoulder IER, elbow FE, SP, wrist RUD, wrist FE, and hand (end effector) respectively. Distance from shoulder to elbow and elbow to wrist are extracted from [25], where 50^{th} percentile data of men were taken.

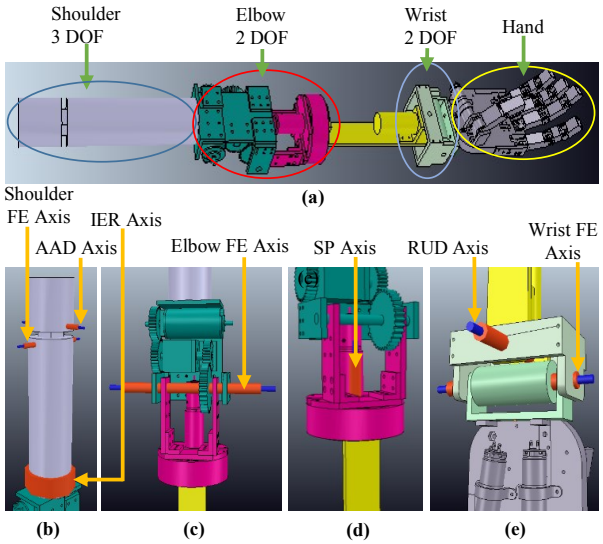

Fig. 2. Simulation environment. (a) Prosthesis and virtual shoulder, (b) Virtual shoulder, (c) Elbow, (d) Forearm, and (e) Wrist

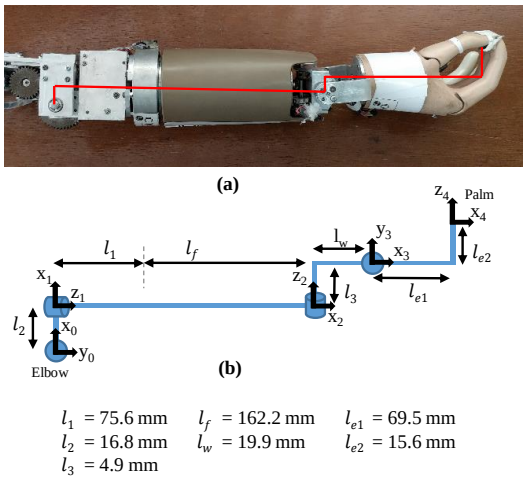

l_1 = 75.6 mm l_f = 162.2 mm l_{e1} = 69.5 mm
l_2 = 16.8 mm l_w = 19.9 mm l_{e2} = 15.6 mm
l_3 = 4.9 mm

Fig. 3. The 5DOF trans-humeral prosthesis. (a) MoBio, (b) Kinematic model. Coordinates frames from frame 0 to frame 4 are attached to the elbow FE, SP, wrist RUD, wrist FE, and hand respectively

signals with EMG signals has been proposed for trans-humeral prostheses.

The proposed task planning method uses a 2-1/2D visual servoing module (VSM) to plan reaching (reach-to-grasp) tasks. An object reaching algorithm is proposed along with the VSM to control the elbow flexion/extension (FE) to drive the palm towards the object of interest. The VSM is integrated with an EMG based module (EBM). The EBM is used to control elbow FE based on a EMG-Force Proportional and Moment Balance model (EFPMB). Since elbow FE has two angular inputs from EBM and VSM, two modules are integrated to get a resultant angle for the elbow FE to reach towards the object of interest while keeping the user controllability.

The paper is organized as follows. Section II depicts the 5DOF prosthesis used for the experimental evaluation of the task planning method. Section III proposes the reach-to-grasp task planning method. Section IV elaborates the results and section V concludes the paper.

II. 5DOF Trans-humeral Prosthesis

A 5DOF trans-humeral prosthesis, MoBio is introduced in this study. The prosthesis was designed considering the bio-mechanics and kinematics of the human upper limb. Human upper limb can be represented as a 7DOF structure with an end effector. The kinematic structure of human upper limb is depicted in Fig. 1.

MoBio is designed to achieve the lost elbow and wrist joints. Moreover, it consists of an 1DOF hand (end effector). A simulation environment and a prototype (MoBio) has been developed using the design of prosthesis.

A. Simulation Environment

The simulation environment is constructed using the Virtual Robotic Experimentation Platform (V-REP) [26], [27]. It consists of a virtual shoulder and the trans-humeral prosthesis. A CAD model of the prosthesis is imported into V-REP and a 3DOF virtual shoulder joint is added to create a complete virtual upper limb with the prosthesis. Thereafter, main joint complexes of the upper limb are modeled in V-REP.

The shoulder joint is modeled as a combination of three revolute joints with mutually perpendicular joint axes. This is equivalent to a standard ball-and-socket joint which consists of shoulder abduction/adduction (AAD), FE, and internal/external rotation (IER). The elbow joint is modeled as two revolute joints: elbow FE and forearm supination/pronation (SP). The wrist is also modeled as two revolute joints with perpendicularly offset axes of rotation for wrist FE and radial/ulnar deviation (RUD). The simulation environment is illustrated in Fig. 2. The virtual shoulder joint of the simulation environment is capable of actuating in accordance with a human shoulder. An Inertial Measurement Unit (IMU) attached to the human shoulder is used to obtain shoulder motions [27].

This article has been accepted for publication in a future issue of this journal, but has not been fully edited. Content may change prior to final publication. Citation information: DOI 10.1109/ACCESS.2017.2727502, IEEE Access

TABLE I
VISION BASED PROSTHETIC CONTROLLERS

Reference	Task	Level of Amputation	DOF	Sensors	Disadvantages	Accuracy
[24]	Estimate grasping pattern (4 types), object size, and orientation of the object to control prosthetic hand accordingly.	Trans-radial	Supination/Pronation and hand DOF.	Web camera, Ultrasonic (US) distance sensor	Lack of sensory feedback.	Size estimation accuracy is higher than 36%.
[16]	Grasp identification (2 types) and control of a bebionic V2 hand prosthesis.	Trans-radial	Hand DOF to adapt two grasping patterns.	Two mechanomyogram (MMG) sensors, web camera.	Lack of grasping types.	Average success rate 84%.
[22]	Estimate grasping pattern (3 types), object size, and object orientation to control a hand prosthesis with wrist rotator.	Trans-radial	Wrist rotation (Supination/Pronation) and hand DOF.	Web camera, US distance sensor, Accelerometer, laser pointer, LED illumination.	Lightning is unnatural for a prosthesis.	Success rate, With lighting 90%, Without lighting 70%.
[21]	Select grasp type (4 types) and size (3 sizes). Triggers using an EMG signal.	Trans-radial	Hand DOF	2 EMG sensors, web camera, US distance sensor, laser pointer.	No closed loop (Look and move) vision control.	Correct type and size 84%. Wrong size, correct type 3%. Correct type, large size 3%.
[23]	Stationary fixed stereo cameras are used to estimate the grasping pattern (4 types) for Electrotherapy.	-N/A-	-N/A-	Two CCD cameras, laser pointer,	Stationary cameras are not suitable for prosthesis applications.	Higher than 90%.

TABLE II
HUMAN AND PROSTHETIC RANGE OF MOTIONS

Motion	Human Limb (Deg)	Prosthesis (Deg)
Shoulder FE	0-53 / 0-153	N/A
Shoulder AAD	0-170	N/A
Shoulder IER	0-70 / 0-90	N/A
Elbow FE	0-146	0-150
Forearm SP	0-84 / 0-71	0-85 / 0-70
Wrist RUD	0-33 / 0-19	0-27 / 0-25
Wrist FE	0-73 / 0-71	0-60 / 0-60

B. MoBio: The 5DOF Trans-humeral Prosthesis

MoBio is the 5DOF trans-humeral prosthesis which has the same mechanism and design as the prosthesis used in the simulation environment. The prosthesis actively powers elbow FE, forearm SP, wrist FE and RUD. The prosthesis is shown in Fig. 3(a). The ranges of motions of the prosthesis is shown in Table II along with the anatomical range of motions of a natural human upper limb.

A kinematic model is developed for the prosthesis to analyze its kinematics (see Fig. 3(b)). Denavit-Hartenberg (DH) parameters relevant to each joint of the MoBio is given in Table III [28]. In Table III, q_1 to q_4 are angles of prosthesis elbow FE, forearm SP, RUD, and wrist FE respectively. θ, d, a, and α are conventional DH notations with the usual meaning. l_e and t_5 are given in (1) and (2) respectively.

$$l_e = \sqrt{l_{e1}^2 + l_{e2}^2} \tag{1}$$

$$t_5 = \tan^{-1}\left(\frac{l_{e2}}{l_{e1}}\right) \tag{2}$$

TABLE III
DH PARAMETERS

Link	θ	d	a	α
1	q_1	0	l_2	$\pi/2$
2	$\pi/2 + q_2$	$l_1 + l_f$	0	$\pi/2$
3	$\pi/2 + q_3$	l_3	l_w	$\pi/2$
4	$t_5 + q_4$	0	l_e	$\pi/2$

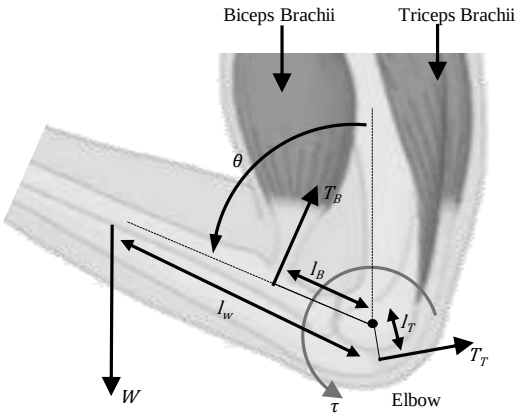

Fig. 4. Forces acting on the forearm. Tendon extending from biceps brachii is connected to the radius bone. It is almost perpendicular to the radius bone. Tendon extending from triceps brachii is connected to the ulnar bone and slides around the elbow joint

III. TASK PLANNING METHOD

The task planning method of the prosthesis consists of two major modules: EBM and VSM. The EBM uses EMG signals of biceps brachii and triceps brachii as inputs to generate elbow FE. VSM uses a camera and a ultrasonic (US) sensor attached to the palm of prosthesis to obtain inputs for planning reach-to-grasp tasks.

This article has been accepted for publication in a future issue of this journal, but has not been fully edited. Content may change prior to final publication. Citation information: DOI 10.1109/ACCESS.2017.2727502, IEEE Access

A. EMG Based Module

EMG based module is based on the EFPMB. EFPMB is proposed to generate elbow motion according to the motion intention of the prosthesis user. It is assumed that a significant portion of biceps brachii and triceps brachii are available after a trans-humeral amputation and the EMG signals generated from amputated muscles can be considered as equivalent to that of a healthy person [29], [30].

The force generated during an isometric contraction is proportional to the EMG signal generated in the respective muscle [31], [32]. Hence, the root mean square (RMS) of EMG signals generated in each muscle is taken as proportional to the force (tension) generated by the muscle. The forces acting on the forearm is modeled as shown in Fig. 4. The elbow angle variation can be modelled as of (3). The detailed derivation can be found in Appendix A.

$$\delta\theta = K_1 E_B - K_2 E_T - K_3 sin(\theta) \tag{3}$$

where, $\delta\theta$, θ, E_B, and E_T are elbow angle change produced by EFPMB, current elbow angle, EMG RMS of biceps brachii, and EMG RMS of triceps brachii, and K_1, K_2, K_3 are proportional constants as given below,

$$K_1 = \frac{M_1 l_B (\delta T)^2}{I} \tag{4}$$

$$K_2 = \frac{M_2 l_T (\delta T)^2}{I} \tag{5}$$

$$K_3 = \frac{W l_W (\delta T)^2}{I} \tag{6}$$

where, δT and I are sample time and moment of inertia of the forearm. M_1 and M_2 are proportional constants to match EMG RMS into muscle force. i.e. Force generated by the biceps brachii is taken as $M_1 E_B$. The RMS is taken for a sample size of 100, sampled at 2000 Hz.

The elbow angle produced by the EFPMB is,

$$\theta_{(t)} = \theta_{(t-1)} + \delta\theta \tag{7}$$

where, $\theta_{(t-1)}$ and $\theta_{(t)}$ are previous elbow angle and elbow angle produced by the EFPMB respectively.

B. Visual Servoing Module

The reach-to-grasp task planning method is developed using the 2-1/2D VSM. The proposed method is capable of altering the orientation of prosthesis to match with the target object orientation while reaching towards an object. The task planning method consists of an image based visual servoing system (IBVS) and a position based visual servoing system (PBVS).

In order to map image features into the end effector velocity of prosthesis, a transformation matrix is used in IBVS. This matrix is known as Image Jacobian matrix. From the end effector of the prosthesis (Cartesian space) to its joint space the inverse kinematics (IK) can be derived. Fig. 5 depicts the IBVS process. The control law is depicted in (8).

$$\dot{q} = -K J^{+} e(f) \tag{8}$$

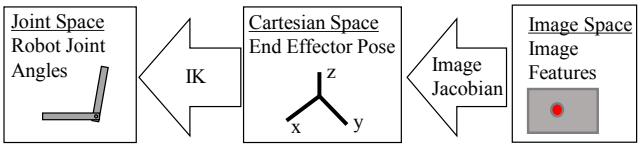

Fig. 5. Image based visual servoing Process. Image features captured using the camera are transformed into the cartesian space using image jacobian. Cartesian space to the robot joints are the inverse kinematics of the robot

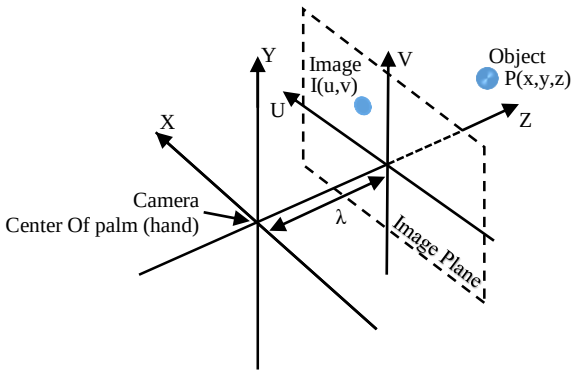

Fig. 6. Perspective projection. Projection of an object in 3D space onto the Camera plane. Image coordinates, (u,v) are extracted from the captured image and object position, (x,y,z) is the actual position of the object with respect to the Camera

where, $\dot{q}$, K, J^{+}, and $e(f)$ are end effector velocity screw ($[V_x, V_y, V_z, \omega_x, \omega_y, \omega_z]^T$), a constant gain, pseudo inverse of Jacobian, and feature error respectively. Jacobian, J can be given as of (9) (refer appendix B) and $e(f)$ can be given as of (10),

$$J = \begin{pmatrix} \frac{\lambda}{z} & 0 & \frac{-u}{z} & \frac{-uv}{z} & \frac{(\lambda^2 u^2)}{\lambda} & -u \\ 0 & \frac{\lambda}{z} & \frac{-v}{z} & \frac{-(\lambda^2+v^2)}{\lambda} & \frac{uv}{\lambda} & u \end{pmatrix} \tag{9}$$

$$e(f) = f_c - f_d \tag{10}$$

where, f_c and f_d are current and desired image features respectively. Current image features are the coordinates of centroid of the object. Desired image features are the center coordinates of the image frame.

Jacobian, J requires the focal length (λ, a fixed parameter of the camera) and distance to the object from the camera, z for the calculation. z is measured using the US sensor attached to the palm of prosthesis.

The desired pose $q_{(t)} = [x, y, z, \alpha, \beta, \gamma]^T$ of the end effector (palm) is calculated as (11) using $\dot{q}$ obtained from (8).

$$q_{(t)} = q_{(t-1)} + \dot{q} \times \delta T \tag{11}$$

where, $q_{(t)}$, $q_{(t-1)}$, and δT are desired pose, current pose, and sample time respectively.

Aforementioned pose is to move the end effector so that the object is in the middle of the image frame. Nevertheless the end effector needs to align with the object, so that the object can be grasped by the hand of the prosthesis (see Fig. 7). This is achieved by combining the IBVS with the PBVS to come

This article has been accepted for publication in a future issue of this journal, but has not been fully edited. Content may change prior to final publication. Citation information: DOI 10.1109/ACCESS.2017.2727502, IEEE Access

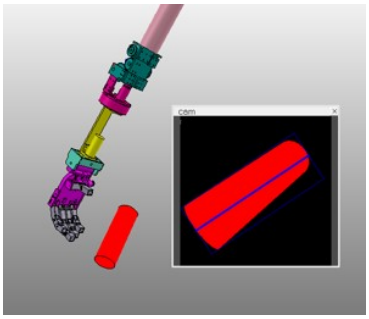

Fig. 7. Misaligned Object. The palm needs to be aligned with the object to grasp the object properly

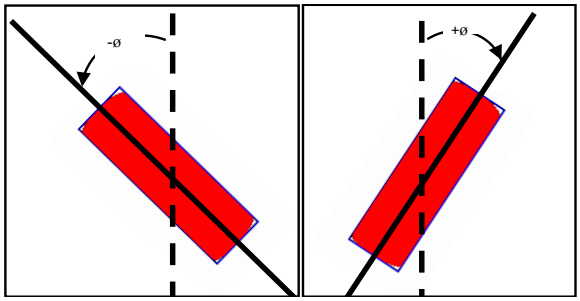

Fig. 8. Misaligned object as seen by camera. Two images of the object as seen by the camera with the misaligned angle, ϕ marked on the images

up with a 2-1/2D VSM. The required angle of rotation along the main axis of camera is calculated using the image. The desired pose of the end effector is transformed from the angle derived, along the camera axis [refer Fig. 8 and (12)].

$$q = q_{(t)} \times T \tag{12}$$

where, q and T are pose after transformation and transformation matrix along the image axis by misaligned angle, ϕ respectively. The sign convention of ϕ is indicated in Fig. 8. Transformation along image axis ($Z - axis$) can be stated as follows.

$$T = \begin{bmatrix} cos(\phi) & -sin(\phi) & 0 & 0 \\ sin(\phi) & cos(\phi) & 0 & 0 \\ 0 & 0 & 1 & 0 \\ 0 & 0 & 0 & 1 \end{bmatrix} \tag{13}$$

The desired joint angles required to achieve the pose, q is derived using an ANN [33]. The VSM is shown in Fig. 9.

The above method is capable of getting the object into middle of the image plane and correct the orientation according to the position and orientation of the hand. However, prosthesis palm may not be able to reach towards the object while keeping the object in the middle of the image plane. In this regard elbow can be treated as the joint which most contributes in making the object closer to the hand. Thus an object reaching algorithm is introduced to adjust the elbow angle and shown in Algorithm 1. It measures the distance to object by rotating it in one direction, if the resultant distance is lower than the previous distance, further rotation in the same direction is performed. Moreover, if the resultant distance is

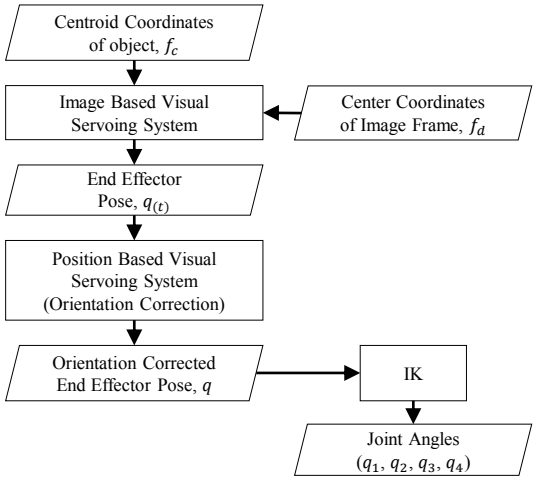

Fig. 9. Visual servoing module. Coordinates of the centroid of object and center coordinates of the image are fed into the IBVS, which gives the palm pose required to center the object in the image frame. Orientation of the palm is corrected by the PBVS

Algorithm 1 Object Reaching Algorithm

state = True ← place holder for two different states
Zto = 0 ← variable for old distance
Zt = 0 ← variable for distance
Dist = 0 ← variable for difference in distance
Ang ← Elbow Angle
L ← Proportional Constant
loop:
while *Zt* <= *50* **do**
    Visual Servoing
    Zto = *Zt*
    Zt ← Measured Depth from US sensor
    Dist = *Zt* - *Zto*
    if *Dist* > 0 **then**
        state = *!state*
    else
        state = *state*
    if *state* == True **then**
        Ang -= (*L* x *Dist*)
    else
        Ang += (*L* x *Dist*)

greater than the previous distance, rotation in other direction is performed.

C. Integration of VSM And EBM

The overall task planning method of the prosthesis is shown in Fig. 10. The task planning method is build integrating the EBM and VSM. The EBM is initially used to move the prosthesis elbow joint according to the human motion intention. A voluntary isometric contraction in biceps brachii and triceps brachii is used to trigger the VSM. The VSM starts servoing towards the object if an object is detected. The joints of prosthesis are controlled using the VSM. However, the elbow has two input angles from the EBM and the VSM. Therefore, a fusion filter is implemented as of Algorithm 2 to

This article has been accepted for publication in a future issue of this journal, but has not been fully edited. Content may change prior to final publication. Citation information: DOI 10.1109/ACCESS.2017.2727502, IEEE Access

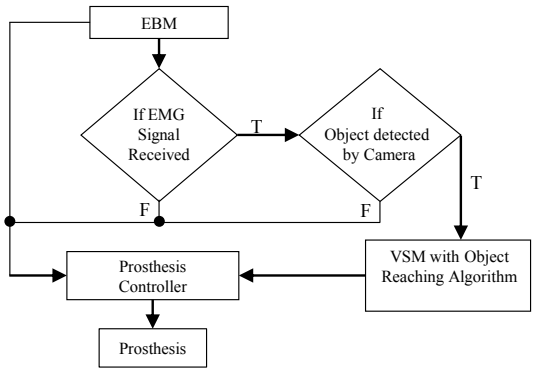

Fig. 10. Overall task planning method of the prosthesis. Initially the elbow FE of the prosthesis is controlled with the EBM. When an object is detected by the camera and the EMG signal is received to reach towards the object, VSM with object reaching algorithm activates and converges towards the object

Algorithm 2 Fusion Filter

state = True ← Place Holder for the VSM state
n = *N* ← Variable for incrementing from 1 to N
$D = 0$ ← Variable for difference between two elbow angles
Th ← Changing Threshold
N ← Number of steps
Ang_{EFE} ← Calculated Elbow angle
Ang_{VS} ← Elbow angle from VSM
Ang_{EMG} ← Elbow angle from EBM
loop:
while $state =$ True **do**
    $D = Ang_{VS} - Ang_{EMG}$
    if $|D| > Th$ **then**
        $n = 1$
    else
        $Ang_{EFE} = Ang_{VS} - Dn/N$
        if $n < N$ **then**
            n += *1*
        else
            n = *N*

control the prosthesis elbow. If the difference of two elbow angles produced by two modules (EBM and VSM) are above the changing threshold, Th The fusion filter goes in to the stepping mode. In stepping mode, the elbow angle changes towards the angle derived from EBM in N steps. However, If the filter is not in the stepping mode the final elbow angle will take the angle from EBM. Both EBM and VSM calculations are running at 50ms intervals (20Hz). N and Th can be set based on the user experience.

IV. Experiments And Results

Experiments are carried out to validate the proposed task planning method. The EBM is evaluated using MoBio. The VSM and the fusion filter are evaluated using the simulation environment.

A. Experimental Setup

The experimental setup is shown in Fig. 11. It consists of the MoBio, EMG acquisition system (Bagnoli 16, Delsys), a

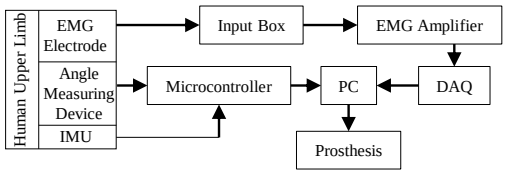

Fig. 11. Experimental setup

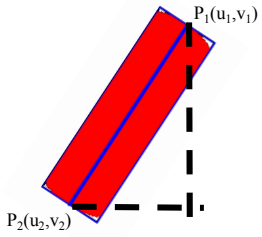

Fig. 12. Detected two points for angle calculation. A bounding rectangle around the detected object is created and two points at the middle of the short edges of the bounding rectangle are selected

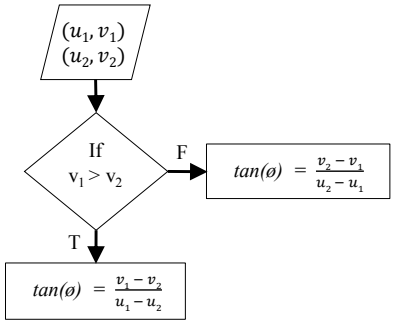

Fig. 13. Calculation of angle, ϕ. Point at the top is selected by comparing v_1 and v_2. Hence the misaligned angle is calculated

personal Computer (PC), IMU, and angle measuring device.

EMG acquisition system is used to extract surface EMG signals from biceps brachii and triceps brachii of 8 healthy subjects. Two single differential EMG sensors are attached on top of the skin surface above biceps brachii and triceps brachii. Sensors are connected to the EMG amplifier through the input box. Amplified EMG signals are transmitted to the PC through a data acquisition (DAQ) card (NI-6220, National Instruments) and processed according to EBM. These signals are sampled at $2000Hz$ and band pass filtered to be within $50Hz$ to $450Hz$. The resultant elbow FE angle is calculated in a Matlab script as of EBM. The calculated elbow FE angle is fed into MoBio using a microcontroller (ATmega2560, Atmel) where the low level joint controllers have been implemented. PC communicates serially (RS232) with the microcontroller at MoBio. EBM experiments are conducted on a real-time basis and subjects are asked to perform elbow FE motion without moving the shoulder. Elbow FE angles of the subject and the MoBio are recorded with two angle measuring devices. These angle measuring devices are equipped with potentiometers and data are recorded using a microcontroller (ATmega2560, Atmel).

In simulations, the joint angles calculated in Matlab are fed

This article has been accepted for publication in a future issue of this journal, but has not been fully edited. Content may change prior to final publication. Citation information: DOI 10.1109/ACCESS.2017.2727502, IEEE Access

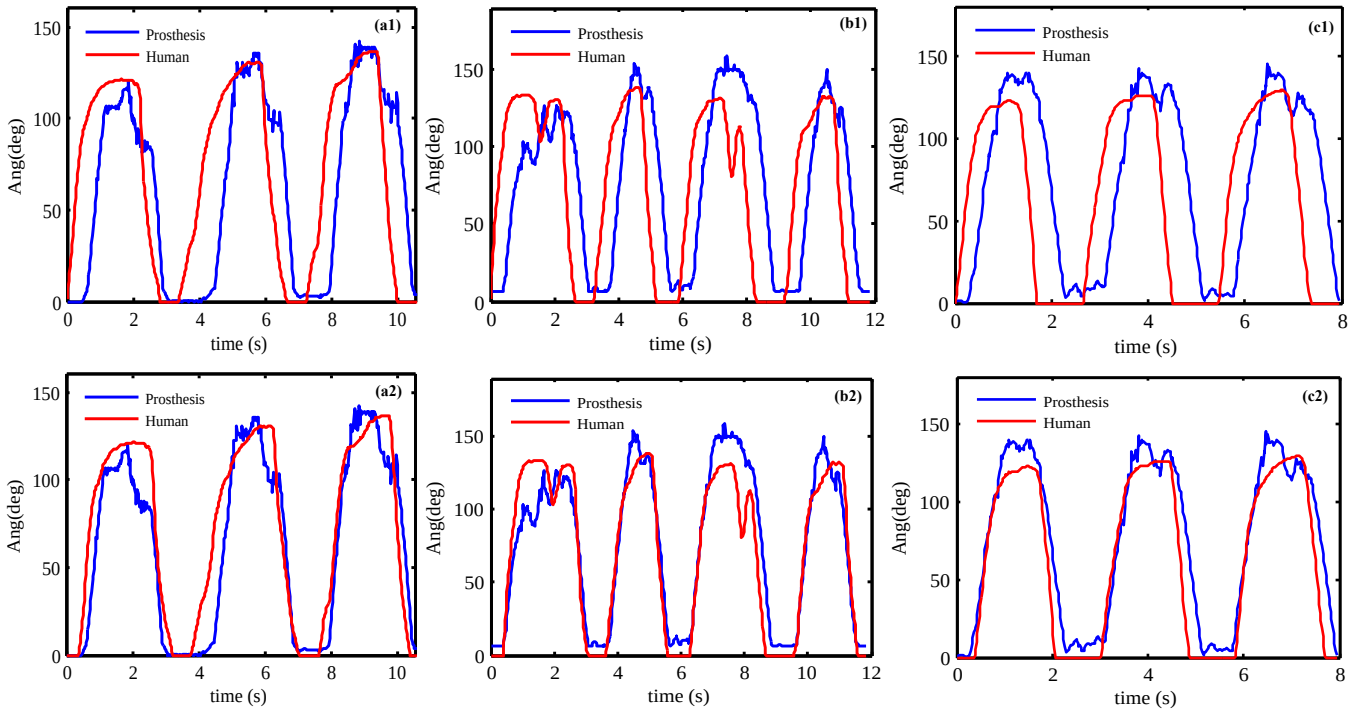

Fig. 14. Comparison of the angle produced by the EBM with the human elbow angle for 3 healthy subjects

TABLE IV
SUMMARY OF EBM PERFORMANCE

Subject	RMSE (Deg)	Time Shift (ms)	RMSE after shift (Deg)
a	24.27	400	11.50
b	28.66	420	10.23
c	29.74	360	10.87
Mean	27.58	396	10.78

into the simulation environment through remote Application Program Interface (API) functionality of V-REP. A virtual camera attached to the palm of the prosthesis is used to identify the target object. Images obtained from the camera are processed using an OpenCV based filter. The filter is capable of detecting objects and returning the centroid image coordinates of the object. These centroid coordinates are processed according to (8) and (11).

The orientation correction process is performed just after visual servoing using the IBVS. The misaligned angle, ϕ is found by identifying two points in the image. These two points are at the two distal ends of the detected object. Those are the center points of the short edges of the constructed bounding rectangle (refer Fig. 12). The angle, ϕ is given as depicted in Fig. 13. This angle is used to calculate the desired pose, q using (12).

Moreover, the fusion filter is also evaluated using the simulation environment. resultant elbow angle calculated from the EBM is fused with the VSM as of fusion filter. The parameters N and Th are found using an user study.

B. Experiments and Results

First the EBM is evaluated. Fig. 14 shows the prosthesis and human angle variation for 3 subjects. In Fig. 14, (a1) and (a2) represents the same result. However, (a1) represents the real-time variation of the elbow angles, in (a2) the prosthesis angle is shifted to the left to match the human elbow angle eliminating the lag. Table IV represents the RMSE, the shifted time or the time lag, and the RMSE after correcting the time lag for the same 3 subjects shown in the Fig. 14. Mean row in Table IV shows the mean values for 8 subjects used for the experiment. The prosthesis follows the desired motion of elbow with an RMSE of 10.78 degrees and percentage error of 7.38% (10.78/146). However, minor lagging behind the actual human limb can be observed due to the processing time incurred and also it takes 50ms to capture signals from the onset of motion. According to literature, a time lag of 300ms is acceptable for real-time operation [34]. Hence, a time lag of 396ms is acceptable and an amputee may get used to this small time lag as he/she uses the prosthesis.

In the second experiment, the IBVS is evaluated. A spherical object is randomly placed on the workspace making it visible to the camera. The convergence of the object towards the center of image frame is observed while changing the shoulder angles from the IMU. The results are shown in Fig. 15. It can be seen from the results that the object goes out from the center of image when the shoulder angles are changed. The IBVS corrects prosthesis angles so that the object converges toward the center again. However, the IBVS alone cannot make the object reach toward the palm. Distance to the object (z) is not reduced to make the object closer to the palm.

In the third experiment, the IBVS with object reaching algorithm is evaluated. The convergence of the palm towards the object is observed. The results are shown in Fig. 16. It can be seen from Fig. 16 that the object converges towards the center of the image frame when the visual servoing is

This article has been accepted for publication in a future issue of this journal, but has not been fully edited. Content may change prior to final publication. Citation information: DOI 10.1109/ACCESS.2017.2727502, IEEE Access

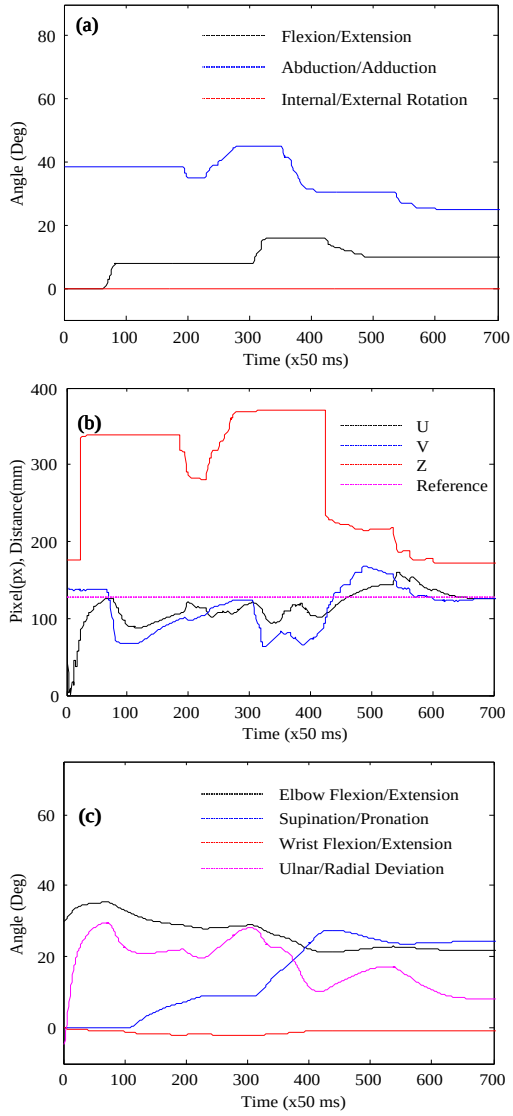

Fig. 15. Reach-to-grasp task planning using IBVS, (a) Shoulder angle variation, (b) Image coordinates and distance to the object variation, and (c) Prosthesis joint angle variation

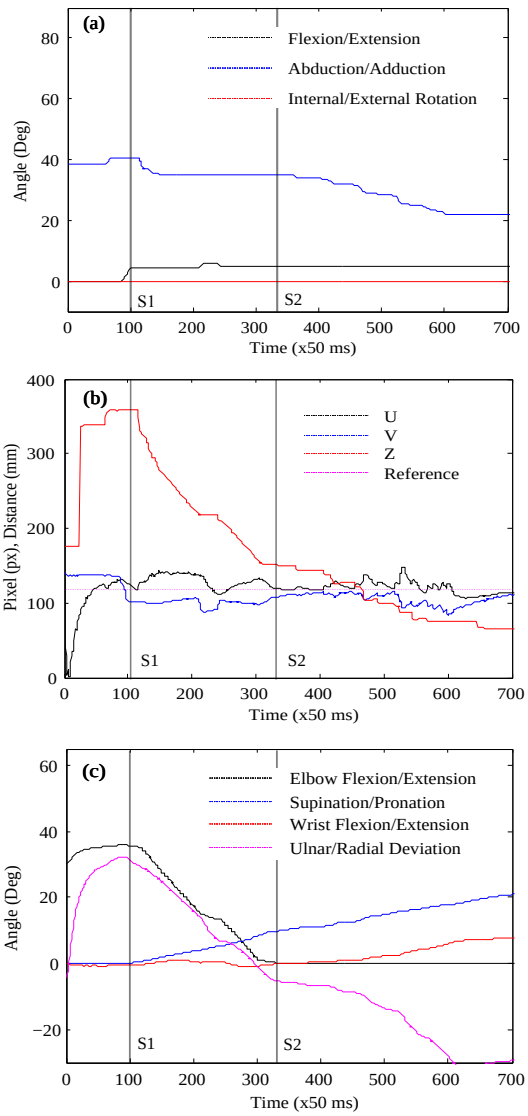

Fig. 16. Reach-to-grasp task planning using IBVS with object reaching algorithm, (a) Shoulder angel variation, (b) Image coordinates and distance to the object variation, and (c) Prosthesis joint angle variation

performed. Moreover, the object reaching algorithm makes the distance to the object minimum by changing the elbow angle as visual servoing is performed. In this process the distance to object (z) is reduced from S1 to S2 time interval [Refer Fig. 16(b)]. The elbow FE angle variation from S1 to S2 time interval to achieve this distance reduction can be seen in Fig. 16(c). From S2 time point onwards, the distance to object (z) is further reduced by changing the shoulder angles. The reaching process by changing the elbow angle is depicted in Fig. 17. z reduces even below 50mm with the help of object reaching algorithm. The experiment is repeated for 10 different object positions. Palm trajectories for 3 of them are shown in Fig. 18. Distance to the object from the palm was 18mm, 23mm, and 28mm respectively for 3 trajectories shown in Fig. 18. As per the palm trajectories, the palm converges towards the object of interest with the aid of object reaching algorithm. The palm trajectory takes a smooth path without any sudden changes despite some curvatures.

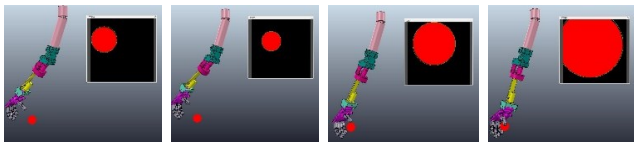

Fig. 17. Reach towards the object of interest by changing the elbow angle using object reaching algorithm

Fourth experiment is the evaluation of PBVS. Only the PBVS is implemented and the resultant image features (position of the centroid and misaligned angle) are recorded. Results are shown in Fig. 19. In the beginning, a cylindrical object misaligned by -10° is placed on the workspace. Fig. 19 shows that the proposed PBVS is capable of correcting the palm orientation so that the object is properly aligned. The PBVS can correct the misaligned angle effectively while keeping the object in the center of image.

Fifth experiment is carried out to evaluate the overall VSM

This article has been accepted for publication in a future issue of this journal, but has not been fully edited. Content may change prior to final publication. Citation information: DOI 10.1109/ACCESS.2017.2727502, IEEE Access

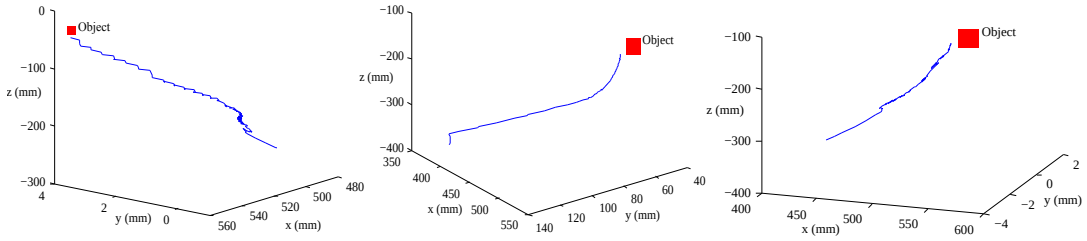

Fig. 18. Palm trajectories for 3 different object positions when reach-to-grasp task planning with object reaching algorithm

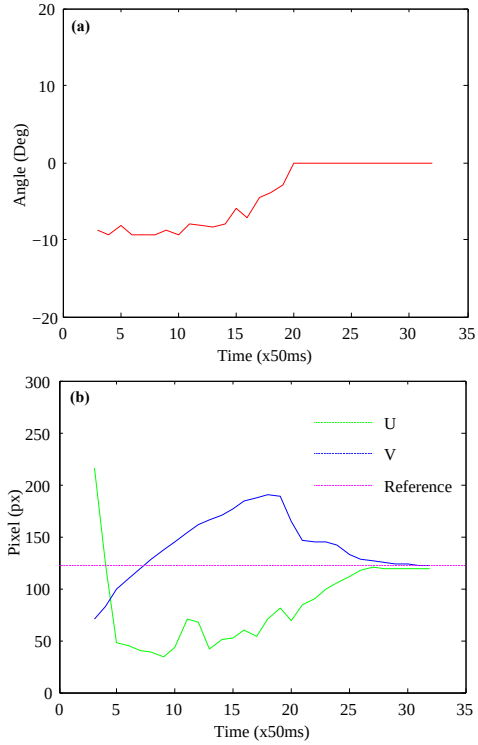

Fig. 19. Correcting palm orientation using PBVS. (a) shows the misaligned angle and (b) shows the image coordinate variation as PBVS is performed

for reach-to-grasp motions of the prosthesis. The orientation of the object is changed between $-10°$ and $10°$ while changing the shoulder angles from IMU. The resultant joint angles from the VSM and the image features are recorded along with the orientation of object and the shoulder angles. Object reaching algorithm is omitted since it may converge the palm towards object preventing further visual servoing. Results are shown in Fig. 20. The PBVS corrects the orientation soon after visual servoing has been performed using IBVS. Orientation correction process causes the object to go out from the center which is then be corrected by the IBVS in the next cycle. The results show that the proposed task planning method is capable of correcting the orientation of the object effectively. Moreover, the object stays within the middle of the image plane.

In the last experiment, the integration of VSM and EBM is evaluated. Two elbow FE angles coming from two modules are used as inputs to the fusing filter. A user study is conducted to decide on the number of steps, N and changing threshold, Th

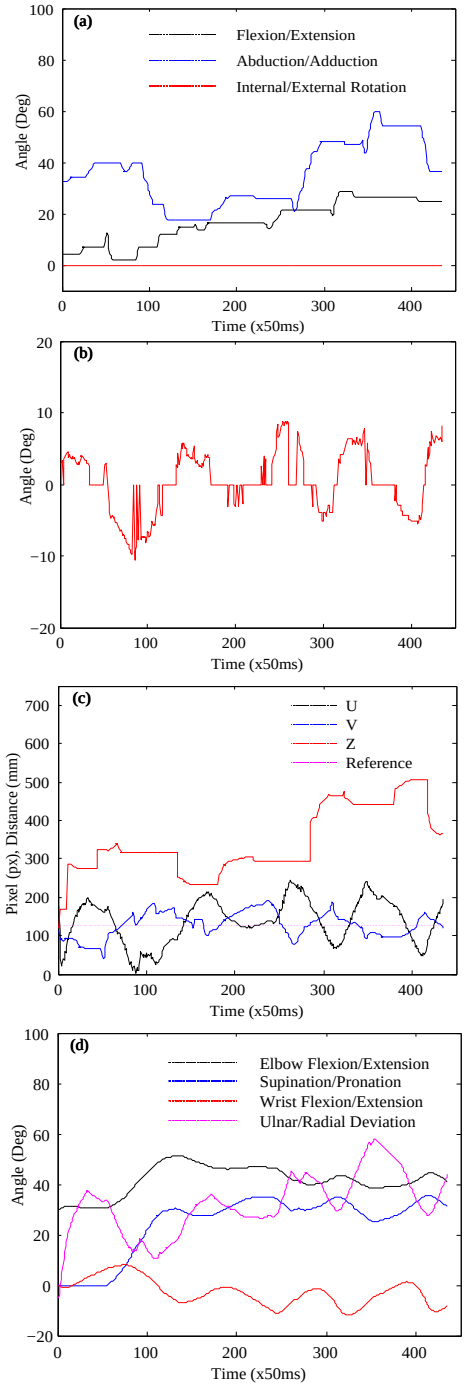

Fig. 20. Reach-to-grasp task planning using overall VSM, (a) Shoulder angle variation, (b) Object orientation as seen by the camera, (c) image coordinate variation, and (d) Prosthesis joint angle variation

This article has been accepted for publication in a future issue of this journal, but has not been fully edited. Content may change prior to final publication. Citation information: DOI 10.1109/ACCESS.2017.2727502, IEEE Access

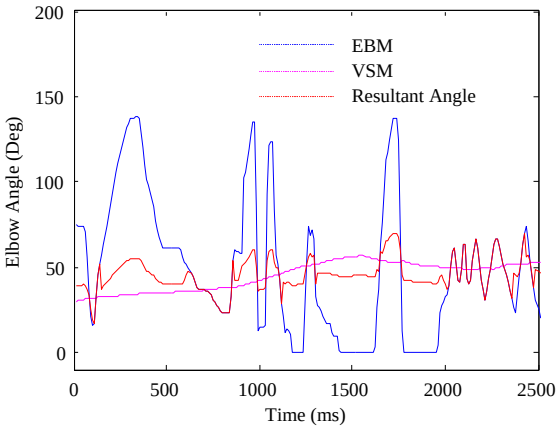

Fig. 21. Resultant elbow FE angle obtained from integrating elbow FE angles derived from VSM and EBM

TABLE V
RESPONSES OF USER STUDY 1

Th (Deg)	No of Responses
4	1
6	2
8	3
10	8
12	4
14	2

for the fusion filter. US1, the first user study is conducted to find the changing threshold, Th. US2, the second user study is conducted to find the number of steps, N. The study is conducted using 20 subjects. In US1, changing threshold is set to different values and users are given the chance to select the best alternative for them. Users are asked to select the minimum elbow angle when the prosthesis should not follow the angle derived from the EBM. The results of US1 is shown in Table. V. In US2, the number of steps, N is set to different values and the subjects are asked to select the best option for them. The subjects are asked to perform a higher elbow angle variation and the fusion filter changes the elbow angle towards the angle derived from the EBM based on the selected N. The responses are given in Table VI. According to the users' responses N and Th are selected, they are 5 and 10° respectively.

The results of the fusion filter are shown in Fig. 21. According to the results, elbow angle follow the VSM. However, when EBM produces slowly varying angles, the elbow angle follows the EBM. Nevertheless, if the EBM produces a sudden angle variation, only a part of that $(1/5)$ is reflected in the final elbow angle. If the EBM angle variation persists, the fusing filter drives the elbow angle towards the angle derived from EBM in 5 steps.

V. CONCLUSION

This paper proposed a hybrid vision based reach-to-grasp task planning method for trans-humeral prostheses. The proposed task planning method is capable of controlling the elbow of the prosthesis with EMG signals using the proposed EFPMB model. Furthermore, this study used a 2-1/2D visual servoing module to center the object relative to the prosthesis palm while aligning the palm with orientation of the object. An object reaching algorithm is proposed for the elbow joint to reach the prosthesis palm towards the object while reducing the distance to the object. Experimental results validated the effectiveness of the proposed hybrid vision based task planning method. EFPMB model was capable of predicting elbow flexion/extension motion with an RMSE of 10.78, percentage error of 7.38% and a real time delay of 400 ms. Additionally, the task planning method was capable of converging towards the object while keeping the controllability through human motion intention. The palm was able to reach towards objects with a distance less than 30mm. The prosthesis elbow followed the EMG based module when the human elbow angle was slowly changed. However, the angle produced by EMG based module does not directly affect the prosthesis elbow angle if EMG based module produces a high difference in angles.

TABLE VI
RESPONSES OF USER STUDY 2

N	No of Responses
2	1
3	2
4	4
5	7
6	3
7	2
8	1

REFERENCES

[1] L. E. Pezzin, T. R. Dillingham, E. J. MacKenzie, P. Ephraim, and P. Rossbach, "Use and satisfaction with prosthetic limb devices and related services 1," *Archives of Physical Medicine and Rehabilitation*, vol. 85, no. 5, pp. 723–729, May 2004.

[2] D. G. K. Madusanka, L. N. S. Wijayasingha, R. A. R. C. Gopura, Y. W. R. Amarasinghe, and G. K. I. Mann, "A review on hybrid myoelectric control systems for upper limb prosthesis," in *Moratuwa Engineering Research Conference*, Apr. 2015, pp. 136–141.

[3] S. Amsuss, P. Goebel, N. Jiang, B. Graimann, L. Paredes, and D. Farina, "Self-Correcting Pattern Recognition System of Surface EMG Signals for Upper Limb Prosthesis Control," *IEEE Transactions on Biomedical Engineering*, vol. 61, no. 4, pp. 1167–1176, Apr. 2014.

[4] J. Liu, "Adaptive myoelectric pattern recognition toward improved multifunctional prosthesis control," *Medical Engineering & Physics*, vol. 37, no. 4, pp. 424–430, Apr. 2015.

[5] A. L. Edwards, M. R. Dawson, J. S. Hebert, C. Sherstan, R. S. Sutton, K. M. Chan, and P. M. Pilarski, "Application of real-time machine learning to myoelectric prosthesis control: A case series in adaptive switching," *Prosthetics and Orthotics International*, Sep. 2015.

[6] S. Amsuess, I. Vujaklija, P. Gobel, A. Roche, B. Graimann, O. Aszmann, and D. Farina, "Context-Dependent Upper Limb Prosthesis Control for Natural and Robust Use," *IEEE Transactions on Neural Systems and Rehabilitation Engineering*, vol. 24, no. 7, pp. 744–753, 2016.

[7] C. J. De Luca, "The use of surface electromyography in biomechanics," *Journal of applied biomechanics*, vol. 13, pp. 135–163, 1997.

[8] E. Criswell, *Cram's introduction to surface electromyography*. Jones & Bartlett Publishers, 2010.

[9] E. Niedermeyer and F. L. da Silva, *Electroencephalography: basic principles, clinical applications, and related fields*. Lippincott Williams & Wilkins, 2005.

[10] T. Pistohl, T. Ball, A. Schulze-Bonhage, A. Aertsen, and C. Mehring, "Prediction of arm movement trajectories from ECoG-recordings in humans," *Journal of neuroscience methods*, vol. 167, no. 1, pp. 105–114, 2008.

[11] D. Farina, N. Jiang, H. Rehbaum, A. Holobar, B. Graimann, H. Dietl, and O. Aszmann, "The Extraction of Neural Information from the Surface EMG for the Control of Upper-Limb Prostheses: Emerging Avenues and

Challenges," *IEEE Transactions on Neural Systems and Rehabilitation Engineering*, vol. 22, no. 4, pp. 797–809, Jul. 2014.

[12] A. E. Schultz and T. A. Kuiken, "Neural Interfaces for Control of Upper Limb Prostheses: The State of the Art and Future Possibilities," *PM&R*, vol. 3, no. 1, pp. 55–67, Jan. 2011.

[13] *Muscles Alive: Their Functions Revealed by Electromyography*, 5th ed. Baltimore: Williams & Wilkins, Jun. 1985.

[14] T. A. Kuiken, L. A. Miller, R. D. Lipschutz, B. A. Lock, K. Stubblefield, P. D. Marasco, P. Zhou, and G. A. Dumanian, "Targeted reinnervation for enhanced prosthetic arm function in a woman with a proximal amputation: a case study," *The Lancet*, vol. 369, no. 9559, pp. 371–380, Feb. 2007.

[15] D. C. Tkach, A. J. Young, L. H. Smith, E. J. Rouse, and L. J. Hargrove, "Real-time and offline performance of pattern recognition myoelectric control using a generic electrode grid with targeted muscle reinnervation patients," *IEEE Transactions on Neural Systems and Rehabilitation Engineering*, vol. 22, no. 4, pp. 727–734, 2014.

[16] M. Gardner, R. Woodward, R. Vaidyanathan, E. Burdet, and B. C. Khoo, "An unobtrusive vision system to reduce the cognitive burden of hand prosthesis control," in *International Conference on Control, Automation, Robotics, And Vision*, Dec. 2014, pp. 1279–1284.

[17] S. Hutchinson, G. D. Hager, P. Corke, and others, "A tutorial on visual servo control," *IEEE Transactions on Robotics and Automation*, vol. 12, no. 5, pp. 651–670, 1996.

[18] F. Chaumette and S. Hutchinson, "Visual servo control. I. Basic approaches," *IEEE Robotics Automation Magazine*, vol. 13, no. 4, pp. 82–90, Dec. 2006.

[19] F. Chaumette, "Visual servoing," in *Computer Vision*. Springer, 2014, pp. 869–874.

[20] F. Janabi-Sharifi, L. Deng, and W. J. Wilson, "Comparison of Basic Visual Servoing Methods," *IEEE/ASME Transactions on Mechatronics*, vol. 16, no. 5, pp. 967–983, Oct. 2011.

[21] S. Došen, C. Cipriani, M. Kostić, M. Controzzi, M. C. Carrozza, and D. B. Popović, "Cognitive vision system for control of dexterous prosthetic hands: Experimental evaluation," *Journal of NeuroEngineering and Rehabilitation*, vol. 7, no. 1, p. 42, 2010.

[22] D. Klisic, M. Kostic, S. Dosen, and D. B. Popovic, "Control of prehension for the transradial prosthesis: Natural-like image recognition system," *Journal of Automatic Control*, vol. 19, no. 1, pp. 27–31, 2009.

[23] M. trbac and M. Markovi, "Stereovision system for estimation of the grasp type for electrotherapy," *Serbian Journal of Electrical Engineering*, vol. 8, no. 1, pp. 17–25, 2011.

[24] S. Doen and D. B. Popovi, "Transradial Prosthesis: Artificial Vision for Control of Prehension," *Artificial Organs*, vol. 35, no. 1, pp. 37–48, Jan. 2011.

[25] A. Freivalds, *Biomechanics of the Upper Limbs: Mechanics, Modeling and Musculoskeletal Injuries, Second Edition*. CRC Press, Feb. 2011.

[26] E. Rohmer, S. P. N. Singh, and M. Freese, "V-REP: A versatile and scalable robot simulation framework," in *IEEE/RSJ International Conference on Intelligent Robots and Systems*, Nov. 2013, pp. 1321–1326.

[27] D. G. K. Madusanka, R. A. R. C. Gopura, Y. W. R. Amarasinghe, and G. K. I. Mann, "A Simulation Environment for Control Algorithms of Transhumeral Prostheses," in *International Conference on Emerging Trends in Mechanical Engineering*, Sep. 2015, pp. 190–196.

[28] P. Corke, "A Simple and Systematic Approach to Assigning Denavit — Hartenberg Parameters," *IEEE Transactions on Robotics*, vol. 23, no. 3, pp. 590–594, Jun. 2007.

[29] P. Shenoy, K. J. Miller, B. Crawford, and R. P. N. Rao, "Online Electromyographic Control of a Robotic Prosthesis," *IEEE Transactions on Biomedical Engineering*, vol. 55, no. 3, pp. 1128–1135, Mar. 2008.

[30] E. Scheme and K. Englehart, "Electromyogram pattern recognition for control of powered upper-limb prostheses: State of the art and challenges for clinical use," *Journal of rehabilitation research and development*, vol. 48, no. 6, pp. 643–660, 2011.

[31] D. Staudenmann, I. Kingma, A. Daffertshofer, D. F. Stegeman, and J. H. van Dieën, "Improving emg-based muscle force estimation by using a high-density emg grid and principal component analysis," *IEEE Transactions on Biomedical Engineering*, vol. 53, no. 4, pp. 712–719, 2006.

[32] A. L. Hof, "The relationship between electromyogram and muscle force," *Sportverletzung Sportschaden: Organ Der Gesellschaft Fur Orthopadisch-Traumatologische Sportmedizin*, vol. 11, no. 3, pp. 79–86, Sep. 1997.

[33] D.G.K. Madusanka, R.A.R.C. Gopura, Y.W.R. Amarasinghe, and G.K.I. Mann, "IBVS and EMG based reach-to-grasp task planning method for a trans-humeral prosthesis," in *IEEE/SICE International Symposium on System Integration*, Dec. 2016, pp. 447–452.

[34] M. Asghari Oskoei and H. Hu, "Myoelectric control systems — A survey," *Biomedical Signal Processing and Control*, vol. 2, no. 4, pp. 275–294, Oct. 2007.

APPENDIX

A. EFPMB Derivation

By considering the moment balance around elbow axis as per the forearm model given in Fig. 4,

$$T_B l_B = \tau + T_T l_T + W l_W sin(\theta) \tag{14}$$

where, τ, T_B, T_T, W, l_B, l_T, l_W, and θ are torque applied on elbow joint, force generated by biceps brachii, force generated by triceps brachii, weight of the forearm, perpendicular distance to T_B from elbow axis, perpendicular distance to T_T from elbow axis, distance to W from elbow axis, and current elbow angle respectively. (14) can be rearranged as follows,

$$I\alpha = T_B l_B - T_T l_T - W l_W sin(\theta) \tag{15}$$

where,

$$\tau = I\alpha \tag{16}$$

where, α and I are angular acceleration and moment of inertia of the forearm respectively.

When discretizing (15), α can be stated as of (17),

$$\alpha = \delta\theta/(\delta T)^2 \tag{17}$$

Hence, by discretizing (15),

$$\delta\theta = \frac{T_B l_B - T_T l_T - W l_W sin(\theta)}{I} \times (\delta T)^2 \tag{18}$$

where, $\delta\theta$ and δT are elbow angle change produced by the EFPMB and sample time respectively.

Assuming EMG RMS is proportional to the force generated by the muscles,

$$T_B = M_1 E_B \tag{19}$$

$$T_T = M_2 E_T \tag{20}$$

where, E_B , E_T, M_1 and M_2 are EMG RMS of biceps brachii, EMG RMS of triceps brachii, and proportional constant for biceps brachii, and proportional constant for triceps brachii respectively.

Since I, δT, W, and l_W are constant and l_B, l_T can be assumed to be constant around 90° of elbow angle, (18) can be stated as,

$$\delta\theta = K_1 E_B - K_2 E_T - K_3 sin(\theta) \tag{21}$$

where, K_1, K_2, and K_3 are proportional constants.

B. IBVS Derivation

End effector velocity ($\dot{P}$) with respect to camera frame can be expressed as of (22).

$$\dot{P} = \omega \times P + V \tag{22}$$

where P, ω, and V are point attached to the end effector, angular velocity of point P, and translational velocity of point P respectively. (22) can be expanded as follows,

$$\begin{pmatrix} \dot{x} \\ \dot{y} \\ \dot{z} \end{pmatrix} = \begin{pmatrix} z.\omega_y - y.\omega_z \\ x.\omega_z - z.\omega_x \\ y.\omega_x - x.\omega_y \end{pmatrix} + \begin{pmatrix} V_x \\ V_y \\ V_z \end{pmatrix} \tag{23}$$

where $[x, y, z]^T$, $[\omega_x, \omega_y, \omega_z]^T$, and $[V_x, V_y, V_z]^T$ are point P, angular velocity of P, and translational velocity of P respectively.

The projection of P onto image plane is taken as $I(u, v)$ (refer Fig. 6). From equations of similar triangles,

$$x = \frac{uz}{\lambda} \tag{24}$$

$$x = \frac{vz}{\lambda} \tag{25}$$

where, λ is the focal length of the camera. By substituting (24) and (25) into (23),

$$[\dot{u}, \dot{v}]^T = J[V_x, V_y, V_z, \omega_x, \omega_y, \omega_z]^T \tag{26}$$

where,

$$J = \begin{pmatrix} \frac{\lambda}{z} & 0 & \frac{-u}{z} & \frac{-uv}{z} & \frac{(\lambda^2 u^2)}{\lambda} & -u \\ 0 & \frac{\lambda}{z} & \frac{-v}{z} & \frac{-(\lambda^2+v^2)}{\lambda} & \frac{uv}{\lambda} & u \end{pmatrix} \tag{27}$$